J. Fluid Mech. (2001), *vol.* 440, *pp.* 269–291. Printed in the United Kingdom

Effect of membrane bending stiffness on the deformation of capsules in simple shear flow

By C. POZRIKIDIS

Department of Mechanical and Aerospace Engineering, University of California, San Diego, La Jolla, California 92093-0411, USA
e-mail: cpozrikidis@ucsd.edu

(Received 11 April 2000 and in revised form 7 February 2001)

The effect of interfacial bending stiffness on the deformation of liquid capsules enclosed by elastic membranes is discussed and investigated by numerical simulation. Flow-induced deformation causes the development of in-plane elastic tensions and bending moments accompanied by transverse shear tensions due to the non-infinitesimal membrane thickness or to a preferred configuration of an interfacial molecular network. To facilitate the implementation of the interfacial force and torque balance equations involving the hydrodynamic traction exerted on either side of the interface and the interfacial tensions and bending moments developing in the plane of the interface, a formulation in global Cartesian coordinates is developed. The balance equations involve the Cartesian curvature tensor defined in terms of the gradient of the normal vector extended off the plane of the interface in an appropriate fashion. The elastic tensions are related to the surface deformation gradient by constitutive equations derived by previous authors, and the bending moments for membranes whose unstressed shape has uniform curvature, including the sphere and a planar sheet, arise from a constitutive equation that involves the instantaneous Cartesian curvature tensor and the curvature of the resting configuration. A numerical procedure is developed for computing the capsule deformation in Stokes flow based on standard boundary-element methods. Results for spherical and biconcave resting shapes resembling red blood cells illustrate the effect of the bending modulus on the transient and asymptotic capsule deformation and on the membrane tank-treading motion.

1. Introduction

The hydrostatics and hydrodynamics of liquid capsules enclosed by thin elastic shells or chemical and biological membranes consisting of molecular networks have received considerable attention in cellular biology, bioengineering, and microencapsulation technology. Fundamental studies have sought to establish the significance of the interfacial mechanical properties on the equilibrium shape, deformability, and transient motion of capsules in various types of flow, and to quantify their effect on the rheology of dilute and concentrated suspensions. Since the interfacial properties are related to the interface thickness or molecular constitution, hydrodynamical diagnostics may be used to probe and ultimately guide the design of capsules with desired properties.

Previous authors have studied the deformation of capsules enclosed by elastic shells of small or infinitesimal thickness using analytical, experimental, and numerical methods. The pioneering theoretical investigations of Barthès-Biesel (1980) and

Barthès-Biesel & Rallison (1981) illustrated the effect of interfacial elasticity on the capsule deformation and on the rheology of dilute suspensions for small deformations from the spherical shape. Numerical studies for moderate and large deformations were subsequently presented by Pozrikidis (1995), Eggleton & Popel (1998), Ramanujan & Pozrikidis (1998), and Navot (1998). Laboratory studies were conducted by Chang & Olbright (1993*a*, *b*), and more recent observations were reported by Walter, Rehage & Leonhard (2000). Other authors incorporated the effects of surface viscosity and incompressibility relevant to biological membranes consisting of lipid bilayers, as reviewed by Pozrikidis (2001).

In addition to viscous, elastic, and isotropic tensions developing to ensure surface incompressibility, capsule interfaces develop bending moments by several physical mechanisms. First, stresses developing over the cross-section of membranes consisting of elastic sheets with non-zero thickness may be integrated over the cross-section to yield stress resultants recognized as tensions, and tangential bending moments accompanied by transverse shear tensions directed normal to the local tangential plane (e.g. Libai & Simonds 1998). Second, molecular membranes composed of three-dimensional proteinic or polymeric networks with fixed connectivity exhibit bending moments due to a preferred three-dimensional unstressed configuration (e.g. Lipowsky 1991). Changes in the solid angles subtended by the bonds raise the potential energy stored in the molecular network and generate bending moments that tend to restore the unstressed configuration. In computational models, the bending energy has been expressed in terms of projections of the unit normal vectors over planar elements defined by three adjacent bonds (e.g. Boey, Boal & Discher 1998; Discher, Boal & Boey 1998). Third, membranes consisting of symmetric thin sheets of amphiphilic molecules favour flat shapes and require energy expenditure to obtain curved shapes (e.g. Lipowsky 1991; Seifert, Berndl & Lipowsky 1991; Seifert 1997).

The development of bending moments endows a shell-like membrane with flexural stiffness whose magnitude may be expressed in terms of a bending modulus that is generally distinct from, and unrelated to, the modulus of elasticity for in-plane deformation. In the absence of bending stiffness, an elastic membrane may wrinkle to develop corrugations with arbitrarily small wavelength under compression. More important, a membrane may fold without resistance to form cornered shapes with small or even vanishing curvature. The presence of bending stiffness imposes limits on the minimum attainable length scale by restricting the minimum radius of curvature above a certain threshold. Steigmann & Ogden (1997, 1999) studied the deformation of membranes coated on the surface of a two- or three-dimensional elastic medium, and concluded that a surface model that does not account for bending stiffness cannot be used to simulate local surface features engendered by the response of solids to compressive surface stress of any magnitude. Although their conclusions apply to deformations of membranes coated on linearly elastic materials, membranes separating viscous fluids are expected to behave in a similar fashion.

Bending stiffness expressed by an appropriate potential energy is believed to play a central role in determining the equilibrium configuration and the shape oscillations of biological membranes consisting of lipid bilayers, including the membrane of red blood cells (Lipowsky 1991). For example, it has long been recognized that, in the absence of bending stiffness, a biconcave capsule is not able to support tensions at equilibrium, and a singularity occurs at the point of extreme axial position (e.g. Fung 1965). The inclusion of bending moments, however small, removes the singular behaviour and allows for tension-bearing interfaces at equilibrium.

The energy of a membrane consisting of a lipid bilayer may be expressed in

terms of a functional involving the distributions of mean and Gaussian curvature multiplied by corresponding bending moduli, as proposed by Canham (1970) and Helfrich (1973), and reviewed by Seifert (1997). At thermal equilibrium, and in the absence of flow-induced deformation, a vesicle enclosed by a membrane assumes a shape with minimum bending energy subject to constraints on the membrane surface area and capsule volume. A variety of stationary and oscillating shapes have been computed based on this formulation using asymptotic and numerical methods. More recently, the analysis has been extended to account for chemical asymmetries in the bilayer and for changes in the molecular surface density due to bending (Seifert 1997).

Our goal in this paper is two-fold. First, to present a formalism that allows the coupling of the membrane to the fluid mechanics in global Cartesian coordinates, and thereby facilitate the theoretical development and the implementation of standard numerical methods for simulating the capsule deformation. Second, to illustrate, in quantitative terms, the effect of bending stiffness on the flow-induced deformation of liquid capsules in Stokes flow, and thereby extend the work of previous authors for membranes that develop only in-plane tensions. The general formulation lends itself to similar problems of flow–structure interaction considered by Pedley, Heil, Luo, and others, as will be discussed in the concluding section.

2. Hydrodynamics and interface mechanics

Consider flow past a capsule containing a viscous fluid labelled 2 and suspended in another fluid labelled 1, as illustrated in figure 1(*a*). The hydrodynamic traction exerted on either side of the interface is denoted, respectively, by $\boldsymbol{f}^{(2)} = \boldsymbol{\sigma}^{(2)} \cdot \boldsymbol{n}$ and $\boldsymbol{f}^{(1)} = \boldsymbol{\sigma}^{(1)} \cdot \boldsymbol{n}$, where $\boldsymbol{\sigma}$ is the hydrodynamic stress tensor, and $\boldsymbol{n}$ is the unit vector normal to the interface pointing outward from the capsule, and the superscripts have the obvious meanings.

The interface is occupied by a membrane that develops anisotropic tensions in the plane of the interface, transverse shear tensions directed normal to the interface, and bending moments in the tangential plane. To balance the resulting interfacial forces, the hydrodynamic traction undergoes a discontinuity across the interface, defined as

$$\Delta \boldsymbol{f} \equiv \boldsymbol{f}^{(1)} - \boldsymbol{f}^{(2)} = \boldsymbol{n} \cdot (\boldsymbol{\sigma}^{(1)} - \boldsymbol{\sigma}^{(2)}). \tag{2.1}$$

Knowledge of the traction discontinuity allows us to compute the instantaneous distribution of the velocity over the interface by solving an integral equation of the second kind,

$$u_i(\boldsymbol{x}_0) = \frac{2}{1+\lambda} u_i^{\infty}(\boldsymbol{x}_0) - \frac{1}{4\pi\mu\,(1+\lambda)} \int_{Interface} G_{ij}(\boldsymbol{x}_0, \boldsymbol{x})\, \Delta f_j(\boldsymbol{x})\, \mathrm{d}S(\boldsymbol{x})$$

$$+ \frac{1-\lambda}{1+\lambda} \frac{1}{4\pi} \int_{Interface}^{PV} u_j(\boldsymbol{x})\, T_{jik}(\boldsymbol{x}, \boldsymbol{x}_0)\, n_k(\boldsymbol{x})\, \mathrm{d}S(\boldsymbol{x}), \tag{2.2}$$

where the point $\boldsymbol{x}_0$ lies at the interface, $\boldsymbol{u}^{\infty}$ is the velocity of a specified externally imposed flow, μ is the viscosity of the ambient fluid, $\lambda\mu$ is the viscosity of the capsule, G_{ij}, T_{ijk} are the velocity and stress Green's functions of the equations of Stokes flow, and PV denotes the principal value of the double-layer integral (e.g. Pozrikidis 1992). Implicit in (2.2) is the assumption that the velocity is continuous across the interface. Having solved the integral equation (2.2), we may evaluate the velocity at any point in the exterior or interior of the capsule using the integral representation of Stokes flow.

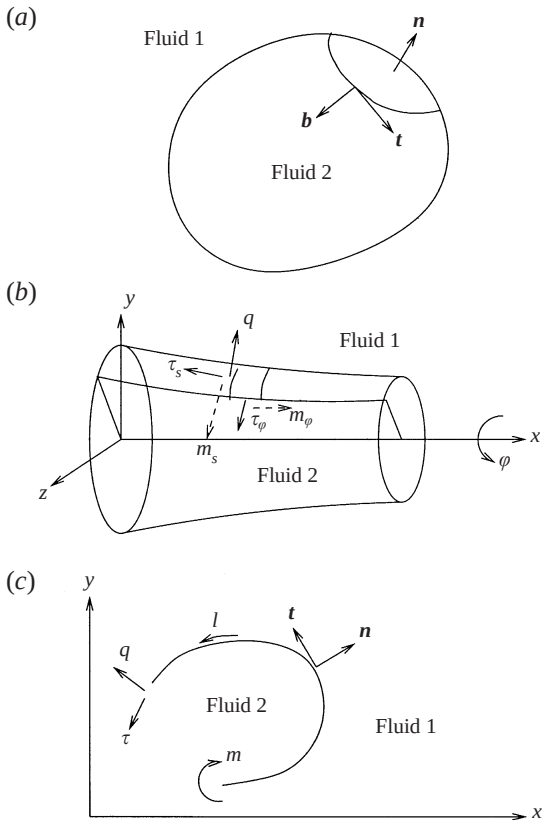

FIGURE 1. Schematic illustration of (*a*) a three-dimensional, (*b*) an axisymmetric capsule, and (*c*) a two-dimensional capsule enclosed by a membrane that develops in-plane elastic tensions, transverse elastic tensions, and elastic bending moments.

The theory of thin shells provides us with a natural framework for modelling the stresses developing over interfaces with a membrane-like constitution of small or infinitesimal thickness. Following the standard formalism, we regard the membrane as a curved two-dimensional medium, and describe its mid-surface in parametric form using two surface curvilinear coordinates (ξ, η) identifying Lagrangian point particles over the interface.

Consider a membrane at a reference configuration Ω_R, and denote the positions of point particles by $\boldsymbol{x}^R(\xi, \eta)$, and the corresponding unit normal vector pointing outward by $\boldsymbol{n}^R(\xi, \eta)$. Assume now that the membrane deforms to a new configuration Ω_t, and denote the new positions of the point particles by $\boldsymbol{x}(\xi, \eta)$, and the corresponding unit normal vector by $\boldsymbol{n}(\xi, \eta)$. The energy stored in the membrane due to the developing tensions and bending moments may be expressed as a surface integral over the reference shape Ω_R involving appropriate measures of strain and bending. The traction discontinuity $\Delta \boldsymbol{f}$ may then be computed in terms of the surface energy using the principle of virtual displacements, as follows (e.g. Valid 1995).

Consider an infinitesimal incremental deformation of the interface from the current configuration Ω_t, corresponding to the infinitesimal energy variation δE. The principle of virtual displacements provides us with an integral equation of the first kind for the

hydrodynamic traction discontinuity,

$$\delta E = \int_{\Omega_t} \Delta \boldsymbol{f} \cdot \delta \boldsymbol{x} \, \mathrm{d}S. \tag{2.3}$$

Assume, for illustration, that the interface energy is equal to the instantaneous surface area S_{Ω_t} multiplied by the uniform surface tension γ. Using results of differential geometry, we find

$$\delta E = \gamma \delta S_{\Omega_t} = \gamma \int_{\Omega_t} 2\kappa_m \boldsymbol{n} \cdot \delta \boldsymbol{x} \, \mathrm{d}S \tag{2.4}$$

where κ_m is the interface mean curvature. Comparing (2.4) with (2.3), we find the well-known relationship for the jump in traction across an interface with constant surface tension, $\Delta \boldsymbol{f} = \gamma \, 2\kappa_m \boldsymbol{n}$.

The solution of (2.3) in the more general case of non-isotropic tension can be found by expanding the dispacement $\delta \boldsymbol{x}(\xi, \eta)$ and traction discontinuity in series of basis functions, and then deriving algebraic equations for the coefficients by linearization. In the simplest approach, the integral on the left-hand side of (2.3) is approximated with a weighted sum over interfacial nodes using the mid-point rule, and variations are considered with respect to infinitesimal displacements of the nodes (Kraus *et al.* 1996). In this case, the traction discontinuity at a node arises directly from the respective variation, and solving an integral equation is not required. Higher-order disretization based on finite-element or boundary-element methods requires solving systems of linear integral equations descending from the integral equation.

As an alternative, the jump in the hydrodynamic traction may be computed directly by balancing the interfacial forces and torques and the rate of change of the interface linear and angular momentum, taking into explicit consideration interfacial tensions, transverse shear tensions, and bending moments. These balances may also be derived by applying the principle of virtual displacements on an infinitesimal interfacial patch, using variations in displacement that express, respectively, rigid-body translation and rotation.

To facilitate the coupling of shell and fluid mechanics, it is desirable to express the membrane tensions and bending moments in global Cartesian coordinates. Global Cartesian formulations have been developed by Valid (1995) for shells of infinitesimal thickness with emphasis on the principle of virtual displacements, and by Libai & Simonds (1998, Chapter VIII) in the more traditional setting of the theory of thin shells. Our first task is to establish a theoretical framework that allows a direct physical intepretation and facilitates numerical computation based on standard numerical methods.

3. Interfacial tensions and bending moments

To develop the global Cartesian formulation, we describe the in-plane tensions developing in the membrane by the Cartesian tensor $\boldsymbol{\tau}$, so that the in-plane tension exerted on a cross-section of the membrane that is normal to the tangential unit vector $\boldsymbol{b}$, as illustrated in figure 1(*a*), is given by $\boldsymbol{b} \cdot \boldsymbol{\tau}$; furthermore, we require $\boldsymbol{n} \cdot \boldsymbol{\tau} = \boldsymbol{0}$ and $\boldsymbol{\tau} \cdot \boldsymbol{n} = \boldsymbol{0}$ to ensure that the tensions lie in the tangential plane. The transverse shear tension is described in terms of the global Cartesian vector $\boldsymbol{q}$, so that the transverse shear tension in the direction of the unit normal vector $\boldsymbol{n}$ exerted on a cross-section of the membrane that is normal to the tangential unit vector $\boldsymbol{b}$ is given by $\boldsymbol{b} \cdot \boldsymbol{q}$; the extension to three dimensions is effected by requiring $\boldsymbol{n} \cdot \boldsymbol{q} = 0$. The complete interface

tension tensor, incorporating tangential and transverse shear tensions, is given by

$$\boldsymbol{T} \equiv \boldsymbol{\tau} + \boldsymbol{q}\boldsymbol{n}. \tag{3.1}$$

The bending moments are expressed in terms of the global Cartesian tensor $\boldsymbol{m}$, so that the moment vector exerted on a membrane cross-section that is normal to the tangential unit vector $\boldsymbol{b}$ is given by $\boldsymbol{n} \times (\boldsymbol{b} \cdot \boldsymbol{m})$; furthermore, to ensure that the bending moments lies in the tangential plane, we require $\boldsymbol{n} \cdot \boldsymbol{m} = \boldsymbol{0}$ and $\boldsymbol{m} \cdot \boldsymbol{n} = \boldsymbol{0}$.

3.1. *Cartesian curvature tensor*

To prepare the ground for deriving interface equilibrium equations and constitutive relations for the bending moments in global Cartesian coordinates, we introduce the Cartesian curvature tensor defined as the gradient of the unit vector normal to the interface pointing outward from the capsule, properly extended off the interface into the three dimensional space,

$$\boldsymbol{B} \equiv \boldsymbol{P} \cdot \nabla \boldsymbol{n}, \tag{3.2}$$

where

$$\boldsymbol{P} \equiv \boldsymbol{I} - \boldsymbol{n}\boldsymbol{n} \tag{3.3}$$

is the tangential projection operator. By definition, and because of the constancy of the length of the unit normal vector,

$$\boldsymbol{n} \cdot \boldsymbol{B} = \boldsymbol{B} \cdot \boldsymbol{n} = \boldsymbol{0}, \tag{3.4}$$

which shows that the normal vector is an eigenvector of $\boldsymbol{B}$ and its transpose with a corresponding zero eigenvalue. The two remaining eigenvectors lie in a plane that is tangential to the interface and are parallel to the mutually orthogonal directions of principal curvature. If $\boldsymbol{e}^{(1)}$, $\boldsymbol{e}^{(2)}$ are the tangential unit eigenvectors, and κ_1, κ_2 are the corresponding principal curvatures, then $\boldsymbol{B}$ can be expressed in the form

$$\boldsymbol{B} = \kappa_1 \boldsymbol{e}^{(1)}\boldsymbol{e}^{(1)} + \kappa_2 \boldsymbol{e}^{(2)}\boldsymbol{e}^{(2)}. \tag{3.5}$$

If the surface is locally spherical, the two principal curvatures are equal to the local mean curvature, $\kappa_1 = \kappa_2 = \kappa_m$, and $\boldsymbol{B} = \kappa_m \boldsymbol{P}$.

The mean curvature of the interface, denoted by κ_m, derives from the trace of $\boldsymbol{B}$ from the relation

$$2\kappa_m = \text{Trace}\,(\boldsymbol{B}), \tag{3.6}$$

which is clearly satisfied when $\boldsymbol{B} = \kappa_m \boldsymbol{P}$. The Gaussian curvature, however, is not related to the determinant of the Cartesian curvature tensor in a simple manner, as it is related to the determinant of the two-dimensional intrinsic curvature tensor defined in terms of derivatives of the normal vector with respect to surface curvilinear coordinates.

To evaluate the curvature tensor $\boldsymbol{B}$ at a point, we consider the variation of the Cartesian components of the position vector $\boldsymbol{x}$ and unit normal vector $\boldsymbol{n}$ along two generally non-orthogonal surface curvilinear coordinates ξ and η, and require

$$\frac{\partial \boldsymbol{n}}{\partial \xi} = \frac{\partial \boldsymbol{x}}{\partial \xi} \cdot \boldsymbol{B}, \quad \frac{\partial \boldsymbol{n}}{\partial \eta} = \frac{\partial \boldsymbol{x}}{\partial \eta} \cdot \boldsymbol{B}. \tag{3.7}$$

Appending to these vector equations the constraint $\boldsymbol{n} \cdot \boldsymbol{B} = \boldsymbol{0}$, we derive three systems of three linear algebraic equations for the three columns of $\boldsymbol{B}$.

3.2. *Interface equilibrium conditions*

Consider a patch of an interface denoted as P, enclosed by a closed loop denoted as C, and a vector or tensor function of position $\boldsymbol{F}$ defined in three-dimensional space. The Gauss divergence theorem provides us with the identity

$$\int_P (\boldsymbol{P}\cdot\nabla)\cdot(\boldsymbol{P}\cdot\boldsymbol{F})\,\mathrm{d}S = \int_C (\boldsymbol{t}\times\boldsymbol{n})\cdot\boldsymbol{F}\,\mathrm{d}l, \tag{3.8}$$

where $\boldsymbol{t}$ is the unit vector that lies in the plane of the interface and is tangential to C. The integrand on the left-hand side of (3.8) is the surface divergence of $\boldsymbol{F}$. If $\boldsymbol{F}$ is normal to the interface, then its suface divergence vanishes.

Assuming now that the mass and thus the inertia of the interface is negligible, we balance the hydrodynamic traction exerted on either side of the interfacial patch with the tensions exerted around the edges, identify $\boldsymbol{F}$ with the complete tension tensor $\boldsymbol{T} = \boldsymbol{\tau} + q\boldsymbol{n}$ defined in (3.1), apply the divergence theorem, and take the limit as the surface area of the patch becomes infinitesimal to derive the differential form of the force equilibrium equation,

$$\Delta\boldsymbol{f} = -(\boldsymbol{P}\cdot\nabla)\cdot(\boldsymbol{\tau}+q\boldsymbol{n}) = -\mathrm{Tr}\,[(\boldsymbol{P}\cdot\nabla)(\boldsymbol{\tau}+q\boldsymbol{n})]. \tag{3.9}$$

The right-hand side of (3.9) is the negative of the surface divergence of the complete interface tension tensor $\boldsymbol{\tau} + q\boldsymbol{n}$.

Performing an analogous torque balance taking into consideration the bending moments exerted around the edges of a selected interfacial patch, we derive an expression for the transverse shear tension vector in terms of the surface divergence of the tensor of bending moments

$$\boldsymbol{q} = [(\boldsymbol{P}\cdot\nabla)\cdot\boldsymbol{m}]\cdot\boldsymbol{P} = \mathrm{Tr}\,[(\boldsymbol{P}\cdot\nabla)\,\boldsymbol{m}]\cdot\boldsymbol{P}, \tag{3.10}$$

and another expression for the antisymmetric part of the in-plane tension tensor

$$\boldsymbol{\tau} - \boldsymbol{\tau}^T = \boldsymbol{B}\cdot\boldsymbol{m} - \boldsymbol{m}^T\cdot\boldsymbol{B}, \tag{3.11}$$

where the supersrcipt T denotes the matrix transpose. The asymmetry of the in-plane tension tensor is due to the effective surface torque field generated by the bending moments and associated transverse shear tensions on a curved interface.

Libai & Simmonds (1998) presented the differential force balance (3.9) in their equation (F.2), p. 460, and derived the differential torque balance in the form

$$\boldsymbol{P}\cdot\nabla\boldsymbol{M}^T = (\boldsymbol{N}\cdot\nabla)\times\boldsymbol{x} \tag{3.12}$$

in their equation (F.6), p. 461. In their notation, $\boldsymbol{N} = \boldsymbol{T}^T$, where $\boldsymbol{T}$ is defined in (3.1). Their bending moment tensor $\boldsymbol{M}$ is related to its more conventional counterpart $\boldsymbol{m}$ by the relation $M_{ij} = \epsilon_{ilk}n_l m_{jk}$. Substituting this relation into (3.12), and decomposing the resulting expression into normal and tangential components, we obtain equations (3.10) and (3.11), thereby confirming the consistency of the present approach.

When the shape of the interface, the elastic tensions, and the bending moments are axisymmetric, as illustrated in figure 1(*b*), the principal directions of $\boldsymbol{\tau}$ and $\boldsymbol{m}$ lie in, or are normal to, a plane of constant meridional angle φ. To simplify the notation, we denote the corresponding elastic tensions by τ_s and τ_φ, and the corresponding bending moments by m_s and m_φ, as illustrated in figure 1(*b*). The vectorial transverse shear tension lies in a meridional plane and is given by $\boldsymbol{q} = q\,\boldsymbol{t}_s$, where $\boldsymbol{t}_s$ is the unit vector tangential to the interface in a meridional plane, and q is the scalar transverse

shear tension. Substituting the expressions

$$\boldsymbol{\tau} = \tau_s \boldsymbol{t}_s \boldsymbol{t}_s + \tau_\varphi \boldsymbol{t}_\varphi \boldsymbol{t}_\varphi, \quad \boldsymbol{m} = m_s \boldsymbol{t}_s \boldsymbol{t}_s + m_\varphi \boldsymbol{t}_\varphi \boldsymbol{t}_\varphi \tag{3.13}$$

into the force equilibrium equation (3.9), and using identities of differential geometry to simplify the resulting equation, we find

$$\Delta \boldsymbol{f} = \left[\kappa_s \tau_s + \kappa_\varphi \tau_\varphi - \frac{1}{\sigma} \frac{\partial}{\partial s}(\sigma q) \right] \boldsymbol{n} - \left[\frac{\partial \tau_s}{\partial s} + \frac{1}{\sigma} \frac{\partial f}{\partial s}(\tau_s - \tau_\varphi) + \kappa_s q \right] \boldsymbol{t}_s, \tag{3.14}$$

where s is the arclength along the trace of the interface in a meridional plane measured in the direction of the tangential unit vector $\boldsymbol{t}_s$, σ is the distance from the x-axis, and the position of the interface is described by the function $\sigma = f(s)$.

Using (3.10), we find that the transverse shear tension is derived from the bending moments by the relation

$$q = \frac{1}{\sigma} \frac{\partial f}{\partial s} \left[\frac{\partial}{\partial \sigma}(\sigma m_s) - m_\varphi \right]. \tag{3.15}$$

Equations (3.14) and (3.15) are in agreement with the classical equations of axisymmetric membrane theory derived in surface curvilinear coordinates (e.g. Timoshenko & Woinowsky-Krieger 1959).

In the case of a two-dimensional interface illustrated in figure 1(c), we obtain the simpler forms

$$\Delta \boldsymbol{f} = -\frac{\partial}{\partial l}(\boldsymbol{\tau} \boldsymbol{t} + q \boldsymbol{n}) = \left[\kappa \boldsymbol{\tau} - \frac{\partial q}{\partial l} \right] \boldsymbol{n} - \left[\frac{\partial \boldsymbol{\tau}}{\partial l} + \kappa q \right] \boldsymbol{t}, \tag{3.16}$$

and

$$q = \frac{\partial m}{\partial l}, \tag{3.17}$$

where l is the arclength measured in the direction of the unit tangent vector $\boldsymbol{t}$, κ is the curvature of the interface in the (x, y)-plane satisfying $\partial \boldsymbol{t}/\partial l = -\kappa \boldsymbol{n}$ and $\partial \boldsymbol{n}/\partial l = \kappa \boldsymbol{t}$, and the rest of the symbols have the obvious meanings.

To compute the jump in the hydrodynamic traction across the interface, $\Delta \boldsymbol{f}$, we require constitutive equations for the in-plane tensions and bending moments in global Cartesian coordinates.

4. Constitutive equations

In the absence of bending moments, the transverse shear stress vanishes and the tensor of the in-plane tensions is symmetric. To develop constitutive equations for finite deformation in global Cartesian coordinates, we follow Barthès-Biesel & Rallison (1981) and consider an infinitesimal interfacial material vector at a reference state and at the deformed state, denoted, respectively, by $\mathrm{d}\boldsymbol{l}^R$ and $\mathrm{d}\boldsymbol{l}$, and introduce the surface deformation gradient defined by the relations

$$\mathrm{d}\boldsymbol{l} = \boldsymbol{F}^S \cdot \mathrm{d}\boldsymbol{l}^R, \quad \boldsymbol{F}^S \cdot \boldsymbol{n}^R = \boldsymbol{n} \cdot \boldsymbol{F}^S = \boldsymbol{0}. \tag{4.1}$$

The second of equations (4.1) ensures that a material vector that is normal to the interface at the reference state is compressed to zero length at the deformed state. The polar decomposition theorem allows the factorization of $\boldsymbol{F}^S$ into the product of an orthogonal matrix $\boldsymbol{R}$ expressing plane rotation, and a symmetric and positive-definite stretch matrix $\boldsymbol{U}$ or $\boldsymbol{V}$, in the form $\boldsymbol{F}^S = \boldsymbol{R}\boldsymbol{U} = \boldsymbol{V}\boldsymbol{R}$. The symmetric and

positive-definite left-hand Cauchy–Green deformation tensor is defined as

$$\boldsymbol{V}^2 = \boldsymbol{F}^S \cdot \boldsymbol{F}^{S^T}. \tag{4.2}$$

One eigenvector of $\boldsymbol{V}^2$ corresponding to zero eigenvalue is normal to the deformed surface, and the remaining two eigenvectors corresponding to the eigenvalues λ_1^2 and λ_2^2 are tangential to the deformed surface.

The in-plane tensions developing in a hyperelastic membrane are derived from a strain-energy function $W(\Lambda_1, \Lambda_2)$ as

$$\boldsymbol{\tau} = \frac{1}{h_S}\left(\frac{\partial W}{\partial \Lambda_1}\boldsymbol{P} + \frac{\partial W}{\partial \Lambda_2}\boldsymbol{V}^2\right), \tag{4.3}$$

where Λ_1 and Λ_2 are two invariants of $\boldsymbol{V}^2$ defined as

$$\Lambda_1 \equiv \log\, h_S = \log(\lambda_1\lambda_2), \quad \Lambda_2 \equiv \tfrac{1}{2}\mathrm{Trace}\,[\boldsymbol{V}^2] - 1 = \tfrac{1}{2}(\lambda_1^2 + \lambda_2^2) - 1, \tag{4.4}$$

and $h_S = \lambda_1\lambda_2$ is the surface areal metric expressing the interfacial dilatation. Equation (4.3) illustrates the symmetry of the in-plane tensions in the absence of bending moments.

For small deformations, the strain-energy function may be approximated with the truncated form

$$W = \tfrac{1}{3}E_S(-\Lambda_1 + \Lambda_2 + \Lambda_1^2), \tag{4.5}$$

where E_S is the surface modulus of elasticity, to be distinguished from the volume modulus of elasticity of a three-dimensional material (Barthès-Biesel & Rallison 1981). The constitutive equation (4.5) will be used in the numerical simulations presented in later sections.

4.1. *Bending moments*

In the presence of bending moments, the in-plane tension tensor $\boldsymbol{\tau}$ is modified with the addition of an antisymmetric component according to equation (3.11), and with the alteration of the symmetric part as required by the functional dependence of the strain energy function on properly defined measures of bending. The reference state of the bending moments, defined as the state where the bending moments vanish, is not necessarily the same as that of the elastic tensions, reflecting differences in the physical mechanisms that are responsible for their respective development. For example, in the case of an interface with a dual molecular structure or a laminated interface consisting of multiple molecular layers or thin shells, the relaxed state of the individual components may correspond to different configurations.

Constitutive equations for elastic tensions and bending moments have been derived by previous authors working in surface curvilinear coordinates (Zarda, Chien & Skalak 1977; Steigmann 1999). One common assumption, also adopted in the present study, is that the bending moments have a negligible effect on the symmetric part of the elastic tensions given in (4.3). Our objective is to develop a Cartesian formulation analogous to that shown in equation (4.3) for the in-plane elastic tensions.

Consider a small material patch of the interface at the resting, and then at a deformed, state. The bending moments developing along the edges of the patch at the deformed state depend on the instantaneous edge curvature, as well as on the edge curvature at the resting state. Evaluation of the latter requires knowledge of the rotation that the edge underwent due to the deformation, and necessitates an involved formulation in terms of the surface deformation gradient (Steigmann & Ogden 1999). If, however, the undeformed surface patch has uniform curvature, knowledge of the

patch rotation is not required: no matter by how much the edge of a material patch has rotated, the curvature of the edge at the undeformed state is constant and independent of orientation.

Motivated by this simplification, we focus our attention on interfaces that are isotropic at the reference bending state. In the case of materially homogeneous and isotropic interfaces, the assumption of isotropy requires that the directional curvature at the reference state is independent of orientation in the tangential plane, which is true for the flat and the spherical shape. For sufficiently small bending deformations, but not necessary small in-plane deformations, the bending moments may be approximated with the linear constitutive equation

$$\boldsymbol{m} = \kappa_B(\Lambda_1, \Lambda_2, \kappa_m, \kappa_G)\,(\boldsymbol{B} - \kappa_m^R \boldsymbol{P}), \tag{4.6}$$

where κ_B is the scalar bending modulus, allowed to be a function of the invariants of the strain and curvature tensors (Steigmann & Ogden 1999), and κ_m^R is the reference mean curvature; κ_m^R is zero for a planar resting shape, and non-zero for a spherical resting shape. Since the bending moment tensor $\boldsymbol{m}$ is symmetric, the antisymmetric part of $\boldsymbol{\tau}$ vanishes, and the bending moments affect only the transverse shear tensions by means of equation (3.11). In the remainder of this paper, we shall assume that κ_B is a physical constant independent of its arguments listed on the right-hand side of equation (4.6).

It is illuminating to compare the constitutive equation (4.6) with those adopted by previous authors for axisymmetric membranes. In the axisymmetric case, knowledge of the principal directions of the in-plane tensions and bending moments allows us to relax the requirement of curvature isotropy at the reference state, and consider non-planar and non-spherical resting shapes. Zarda *et al.* (1977) introduced the bending measures of strain

$$K_s \equiv \lambda_s \kappa_s - \kappa_s^R, \quad K_\varphi \equiv \lambda_\varphi \kappa_\varphi - \kappa_\varphi^R, \tag{4.7}$$

and invoked an analogy with the linear theory of bending of thin plates to derive the following expression for the bending moments:

$$m_s = \frac{\kappa_B}{\lambda_\varphi}(K_s + \nu K_\varphi), \quad m_\varphi = \frac{\kappa_B}{\lambda_s}(K_\varphi + \nu K_s), \tag{4.8}$$

where ν is the Poisson ratio. If the membrane consists of a thin layer of a three-dimensional elastic solid of thickness h, then $\kappa_B = Eh^3/[12(1-\nu^2)]$; for an incompressible material, $\nu = 1/2$. The bending measures of strain (4.7) have been designed so that shape-preserving deformations do not induce bending moments; an example is the deformation of an expanding spherical shell. The bending measures (4.8) are appropriate for molecular membranes whose bending moments depend on the solid angles subtended by molecular networks, but not for membranes consisting of thin sheets of an elastic material whose thickness changes as a result of the deformation. The constititutive equation (4.8) for axisymmetric deformation is a generalization of the more restrictive constitutive equation (4.6), but its applicability to axisymmetric shapes is an important limitation.

Now, given a strain energy function that incorporates the effect of bending moments in terms of bending measures of strain, we may use the principle of virtual displacements to compute the jump in traction across the membrane by solving an integral equation, as discussed in § 2. We may then invert the force balance (3.9) to obtain the in-plane and transverse shear tensions, and finally use the normal component of the torque balance expressed by (3.10) to obtain the bending moments. The

procedure is illustrated by Navot (1998) for membranes developing in-plane elastic tensions where the strain-energy function is defined in terms of the square of the surface divergence of the surface deformation gradient.

The inverse problem, finding the strain-energy function that corresponds to the stipulated constitutive equation (4.6), is more subtle. The linear dependence of the bending moment tensor on the Cartesian curvature tensor suggests that the underlying strain energy function is related to the Helfrich (1973) bending energy functional for biological membranes, given by

$$E \equiv 2\kappa_B \int (\kappa_m - \kappa_m^R)^2 \, \mathrm{d}S + \kappa_B' \int \kappa_G \, \mathrm{d}S, \tag{4.9}$$

where the integration is performed over the *instantaneous* interface, κ_m^R is the spontaneous curvature, which is the counterpart of the reference curvature in our terminology, κ_B is the bending modulus associated with the mean curvature, and κ_B' is the bending modulus associated with the Gaussian curvature. The Gauss–Bonnet theorem states that the last term on the right-hand side of (4.9) is a constant dependent only on the topological genus of the membrane.

To investigate the relationship between the Helfrich energy functional (4.9) and the constitutive equation (4.6), we consider a two-dimensional *inextensible* membrane with vanishing reference curvature, as illustrated in figure 1(*c*). Setting $\kappa_m = \frac{1}{2}\kappa$, where κ is the curvature of the membrane in the (x, y)-plane, we obtain

$$E \equiv \tfrac{1}{2}\kappa_B \int \kappa^2 \, \mathrm{d}l = \tfrac{1}{2}\kappa_B \int \frac{\partial^2 \boldsymbol{x}}{\partial l^2} \cdot \frac{\partial^2 \boldsymbol{x}}{\partial l^2} \, \mathrm{d}l, \tag{4.10}$$

where $\boldsymbol{x}$ is the position of point particles along the membrane, and l is the arclength. Requiring that the arclength between any two point particles is preserved during the deformation, we find that the energy variation due to a virtual displacement $\delta\boldsymbol{x}$ is given by

$$\delta E = \kappa_B \int \left[\frac{\partial^2 \boldsymbol{x}}{\partial l^2} \cdot \frac{\partial^2 \delta \boldsymbol{x}}{\partial l^2} \right] \mathrm{d}l. \tag{4.11}$$

Integrating by parts, we derive the preferred form

$$\delta E = -\kappa_B \int \frac{\partial}{\partial l} \left[\kappa^2 \boldsymbol{t} + \frac{\partial \kappa}{\partial l} \boldsymbol{n} \right] \cdot \delta \boldsymbol{x} \, \mathrm{d}l. \tag{4.12}$$

where $\boldsymbol{t}$ is the unit tangent pointing in the direction of increasing arc length. The inextensibility condition requires that the virtual displacement is subject to the constraint $\boldsymbol{t} \cdot (\partial \delta \boldsymbol{x})(\partial l) = 0$, and this suggests the identity $\int (\partial/\partial l)[f(l)\boldsymbol{t}] \cdot \delta \boldsymbol{x} \, \mathrm{d}l$, where $f(l)$ is an arbitrary function. Comparing (4.12) to (2.3), (3.16), and (3.17), we find $m = \kappa_B \kappa$, in agreement with (4.6). An analogous deduction for the tension is prevented by the integral constraint stated previously in this paragraph.

5. Numerical method

A boundary element method was implemented to simulate the deformation of a capsule from a specified initial shape, including the effect of bending stiffness. The numerical procedure is an extension of that developed by Ramanujan & Pozrikidis (1998) for capsules enclosed by membranes that develop only in-plane elastic tensions. In the numerical implementation, the membrane was discretized into a network of six-node curved triangles generated by successively subdividing a regular octahedron

into descendant elements. When the viscosity ratio λ had a value other than unity, the integral equation (2.2) was solved by the method of successive substitutions, and the surface nodes were convected with the computed fluid velocity.

New features of the numerical procedure include a module for computing the Cartesian curvature tensor $\boldsymbol{B}$ at the nodes of each curved triangle using the local triangle parametric representation written in terms of the triangle barycentric coordinates (ξ, η). First, the normal vector was computed at each node and its components were averaged over the elements sharing the node. Second, the derivatives with respect to ξ and η in equations (3.7) were computed by analytical differentiation assuming that the averaged normal vector and position vector vary quadratically over each element. The components of $\boldsymbol{B}$ were then averaged over the elements sharing the node to improve the accuracy, and the curvature tensor was replaced by its symmetric component to screen out numerical error. Once the curvature tensor was available, the tensor of bending moments $\boldsymbol{m}$ was evaluated from the constitutive equation (4.6).

To evaluate the surface divergence of $\boldsymbol{m}$, we first compute its gradient denoted by $\boldsymbol{J} \equiv (\boldsymbol{P} \cdot \nabla)\boldsymbol{m}$, using the relations

$$\frac{\partial \boldsymbol{m}}{\partial \xi} = \frac{\partial \boldsymbol{x}}{\partial \xi} \cdot \boldsymbol{J}, \quad \frac{\partial \boldsymbol{m}}{\partial \eta} = \frac{\partial \boldsymbol{x}}{\partial \eta} \cdot \boldsymbol{J}, \quad \boldsymbol{n} \cdot \boldsymbol{J} = \boldsymbol{0}. \tag{5.1}$$

The derivatives of the components of the bending moment tensor with respect to ξ and η were computed by analytical differentiation assuming quadratic variation over each element. The evaluation of $\boldsymbol{J}$ at each node of each triangle requires solving nine systems of 3×3 linear equations. The components of $\boldsymbol{J}$ were then averaged over the elements sharing the node to improve the accuracy, and the transverse shear tension followed from the trace of $\boldsymbol{J}$, as shown in equation (3.10).

To compute the single-layer integral over an element shown on the right-hand side of (2.2), we first apply the trapezoidal rule to express it in the approximate form

$$\int_{Element} G_{ij}(\boldsymbol{x}_0, \boldsymbol{x}) \Delta f_j(\boldsymbol{x}) \, \mathrm{d}S(\boldsymbol{x}) \simeq \overline{\Delta f_j} \int_{Element} G_{ij}(\boldsymbol{x}_0, \boldsymbol{x}) \, \mathrm{d}S(\boldsymbol{x}), \tag{5.2}$$

where

$$\overline{\Delta \boldsymbol{f}} \equiv \frac{1}{S_E} \int_{Element} \Delta \boldsymbol{f}(\boldsymbol{x}) \, \mathrm{d}S(\boldsymbol{x}) \tag{5.3}$$

is the average value of the traction discontinuity over the element, and S_E is the surface area of the element. Substituting the right-hand side of (3.9) into the integrand of (5.3), and using the surface divergence theorem, we find

$$\overline{\Delta \boldsymbol{f}} = -\frac{1}{S_E} \int_{Element} [\boldsymbol{b} \cdot \boldsymbol{\tau} + (\boldsymbol{b} \cdot \boldsymbol{q})\boldsymbol{n}](\boldsymbol{x}) \, \mathrm{d}l(\boldsymbol{x}), \tag{5.4}$$

where l the arclength along the element contour, $\boldsymbol{b} \equiv \boldsymbol{t} \times \boldsymbol{n}$ is the unit vector tangential to the element, perpendicular to the unit tangent vector $\boldsymbol{t}$ along the element contour, and orthogonal to the surface unit normal vector $\boldsymbol{n}$.

In the numerical simulations, we consider capsules with spherical and spheroidal initial shapes, and capsules with axisymmetric biconcave shapes resembling the resting shapes of red blood cells. In cylindrical polar coordinates with axial position x and distance from the x-axis denoted by σ, the biconcave shape is described by the equation

$$x(\sigma) = \pm \tfrac{1}{2} R_0 \, (1 - \hat{\sigma}^2)^{1/2} (0.207 + 2.003 \hat{\sigma}^2 - 1.123 \, \hat{\sigma}^4), \tag{5.5}$$

where $\hat{\sigma} \equiv \sigma / R_0$, and R_0 is the maximum radius of the biconcave disk occurring in

the $x = 0$ plane. The average value of R_0 of a healthy red blood cell is close to 3.91 μm, the cell volume is close to $V_c = 1.574R_0^3$, and the membrane surface area is close to $S_c = 8.772R_0^2$ (e.g. Evans & Fung 1972; Fung 1981).

All simulations were conducted with a standard grid of 512 elements defined by 1026 surface nodes located at the vertices and at the mid-points of the edges of the triangles. Tests of accuracy showed that halving the number of elements changes the coordinates of the marker points deployed over deforming capsules with compact shapes by less than 2%. At high deformations, however, significant inaccuracies and numerical instabilities due to inadequate spatial resolution arise. The development of bending moments requires very small time steps for numerical stability, much lower than those necessary to prevent instabilities in the case of membranes that develop only in-plane elastic tensions. Given the strong constraint for stability, time integration was carried out by the explicit Euler method using a constant time step. Geometrical reflection symmetry with respect to the (x, y)-plane was exploited to reduce the cost of the simulations.

Figure 2(*a*) shows stages in the evolution of the trace of the membrane of an initially spheroidal capsule with axes ratios 1:2:2 in the (x, y)-plane, at a sequence of dimensionless times $\hat{t} \equiv t\kappa_B/(\mu a_{eq}^3)$, represented by the circles and connecting solid lines. A caret above x and y indicates that the spatial coordinates have been reduced with respect to the equivalent volume capsule radius. Figure 2(*b*) shows corresponding stages in the evolution of a biconcave disk. In both cases, the viscosity ratio λ is equal to unity, and the modulus of elasticity E_S was set equal to zero. The reference shape of the membrane is a flat sheet with vanishing reference curvature, $\kappa_m^R = 0$, and the motion is driven by bending moments developing due to variations in the membrane curvature.

The simulations shown in figure 2 confirm that the capsule relaxes to the spherical shape whereupon a uniform and isotropic distribution of bending moments and corresponding vanishing tranverse shear tensions are established. In both cases, the capsules remain axially symmetric within the numerical error due to the three-dimensional discretization. To illustrate the time scale of the motion, in figure 2(*c*) we display the evolution of the x- and σ-axes of the relaxing spheroid shown in figure 2(*a*), respectively denoted by a and b, and the corresponding evolution of the Taylor deformation parameter $D_{xy} \equiv |a - b|/(a + b)$. At long times, the spheroid axes tend to the equivalent capsule radius a_{eq}, and the deformation parameter tends to zero.

The simulations presented in figure 2 were conducted with dimensionless time step $\Delta\hat{t} \equiv \Delta t a_{eq}\mu/\kappa_B = 0.0005$. Each run required 1500 time steps at a cost of 12 hours of CPU time on a 550 MHz Intel processor running LINUX with the g77 FORTRAN compiler. Numerical instabilities are discernible at the late stages of the motion displayed in the figures, requiring an even smaller time step to follow the asymptotic approach to the stationary spherical shape. The change in the volume of a capsule due to numerical error was less than 0.01%, which is typical of all simulations presented in the next section. Simulations for non-unit values of λ require a CPU time on the order of several days on the aforementioned computing facility.

A numerical method was also implemented for simulating the evolution of axisymmetric capsules, where axial symmetry is embedded in the mathematical formulation and numerical method (Kwak & Pozrikidis 2001). The method uses the boundary-integral formulation for axisymmetric Stokes flow, where the velocity is expressed in terms of line integrals over the trace of the interface in a meridional plane (e.g. Pozrikidis 1992). The scalar transverse shear tension q was computed by numerical

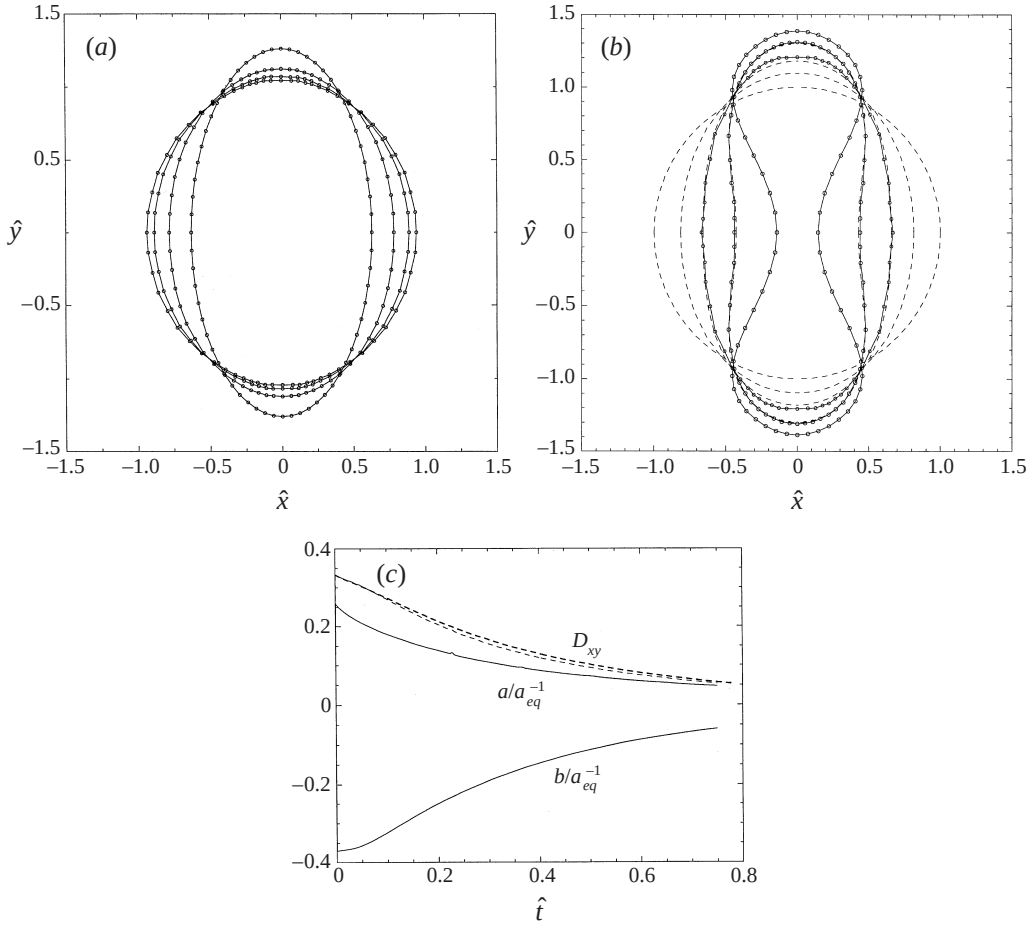

FIGURE 2. (*a*) Relaxation of an initially oblate spheroidal capsule with axes ratio 1:2:2 towards the spherical shape, under the influence of bending moments alone: traces of the interface in the (x, y)-plane at dimensionless times $\hat{t} \equiv t\kappa_B/(\mu a_{eq}^3) = 0$, 0.25, 0.50, 0.74. The viscosity ratio λ is equal to unity, and the reference state of the membrane is the flat sheet. (*b*) Corresponding relaxation of a biconcave disk at times $\hat{t} = 0, 0.25, 0.49, 0.75, \infty$. The circles and connecting solid lines show results obtained using the numerical method for three-dimensional flow, and the dashed lines show results obtained using the numerical method for axisymmetric flow. Numerical instabilities prevented the continuation of the former simulation at long times. (*c*) Evolution of the x- and σ-axes and Taylor deformation parameter of the relaxing spheroid shown in (*a*); the heavy dashed line shows results for the Taylor deformation parameter obtained using the numerical method for axisymmetric flow.

differentiation with respect to radial distance from the x-axis, as required by the right-hand side of equation (3.15). The traction discontinuity was computed from the force balance (3.14).

Because the integration in the direction of the meridional angle is done analytically, the code for axisymmetric flow is significantly more efficient, and produces results that are more accurate than those for three-dimensional flow. Results obtained using the code for axisymmetric flow are shown with the dashed lines in figure 2(*b*), and with the heavy dashed line in figure 2(*c*). In these simulations, the bending moments were computed using the simplified version of the constitutive equation for axisymmetric flow, equation (4.6) whose scalar components are given by equations (4.8) and (4.9), where the stretch ratios are replaced by unity and the Poisson ratio ν is set equal to

zero on the right-hand sides. The good agreement corroborates the consistency of the global Cartesian formulation and testifies to the reliability of the numerical method for three-dimensional flow.

6. Results and discussion

At the initial instant, a capsule with a specified resting shape is exposed to simple shear flow along the x-axis varying along the y-axis with velocity $\boldsymbol{u}^{\infty} = (ky, 0, 0)$, where k is the shear rate. Non-dimensionalizing all variables using as length scale the equivalent volumetric capsule radius a_{eq}, time scale the inverse shear rate k^{-1}, and stress μk, we find that the deformation of the capsule is determined by two parameters: the dimensionless shear rate $G \equiv \mu k a_{eq}/E_S$, and the reduced ratio of the bending modulus to the elastic modulus, $\hat{\kappa}_B \equiv \kappa_B/(a_{eq}^2 E_S)$.

6.1. *Spherical capsules*

The results presented in this section correspond to membranes with flat resting shapes concerning the bending moments, corresponding to vanishing reference curvature. Membranes with non-zero reference curvature were found to behave in a similar fashion.

The simulations reveal that spherical capsules deform and reach stationary shapes, no matter how strong the shear flow, in agreement with the results of previous authors, as reviewed in the Introduction. As expected, bending stiffness restricts the overall capsule deformation and prevents the development of highly curved shapes. Figure 3(a) shows a family of contours of stationary deformed capsules in the (x, y)-plane for viscosity ratio $\lambda = 1$, and reduced bending modulus $\hat{\kappa}_B = 0, 0.01, 0.025$, and 0.0375, at the low shear rate $G = 0.05$. Figure 3(b) shows a family of substantially more deformed contours for $\lambda = 1$, $\hat{\kappa}_B = 0, 0.04, 0.10$, and 0.15, at the higher shear rate $G = 0.20$. The shapes for $\hat{\kappa}_B = 0$ are in excellent agreement with those presented by previous authors including Ramanujan & Pozrikidis (1998); because the numerical method was implemented afresh with various alterations and improvements, the comparison is not entirely contrived. The rounding of the membrane at the tips even for small modulus of bending is evident from these illustrations.

Figure 4 illustrates, in quantitative terms, the effect of bending stiffness on the capsule deformation and orientation. The graphs in figure 4(a, b) show the evolution of the Taylor deformation parameter $D_{xy} = (A - B)/(A + B)$, where A and B are, respectively, the maximum and minimum size of the contour of the capsule in the (x, y)-plane, for $G = 0.05$ and 0.20. The graphs in figure 4(c, d) show the evolution of the inclination angle measured from the x-axis up to the location of the maximum dimension A, denoted by θ_{xy}. The thickness of the lines scales with the magnitude of the modulus of bending. High computational cost for the highest bending modulus has limited the duration of the simulation. The results for $\hat{\kappa}_B = 0$ are in excellent agreement with those presented by Ramanujan & Pozrikidis (1998). In the presence of bending moments, the asymptotic approach to steady state occurs through a mild oscillation possibly due to numerical error which, however, could have been eliminated by computing the deformation parameter based on integral geometrical surface measures, as discussed by Ramanujan & Pozrikidis (1998).

When a capsule has deformed and reached an equilibrium shape, the membrane continues to rotate in a tank-treading mode with period T. The numerical results showed that raising the bending modulus reduces the capsule deformation and shifts

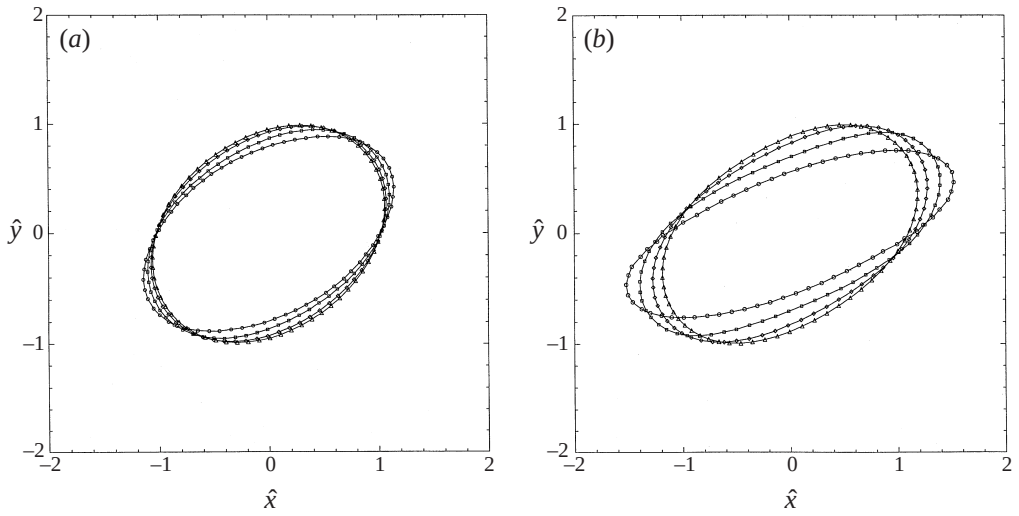

FIGURE 3. Contours of deformed stationary capsules with spherical initial shapes, for $\lambda = 1$, and reduced modulus of bending $\hat{\kappa}_B = 0$, 0.01, 0.025, and 0.0375, at the low dimensionless shear rate $G = 0.05$. (*b*) Corresponding contours for $\hat{\kappa}_B = 0$, 0.044, 0.10, and 0.15, at the higher dimensionless shear rate $G = 0.20$.

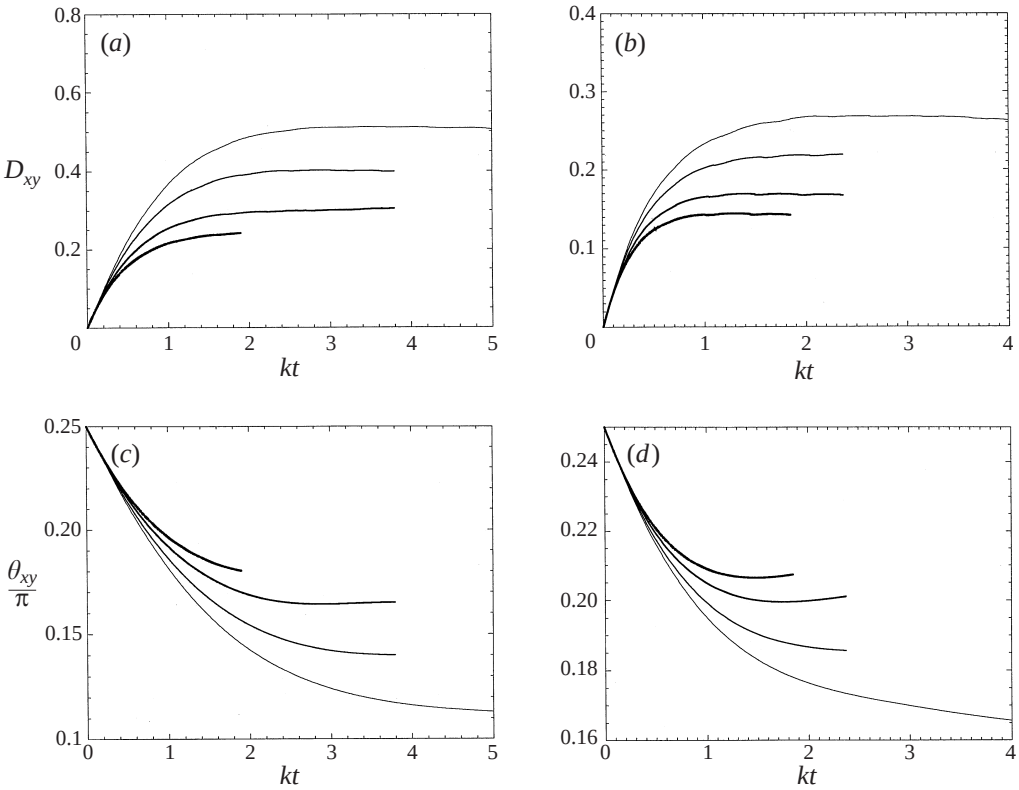

FIGURE 4. (*a*, *b*) Evolution of the Taylor deformation parameter D_{xy} leading to the equilibrium shapes shown in figure 3(*a*, *b*), respectively, for $G = 0.05$ and 0.20. (*c*, *d*) Associated evolution of the inclination angle θ_{xy}. The thickness of the lines increases as the bending modulus is raised.

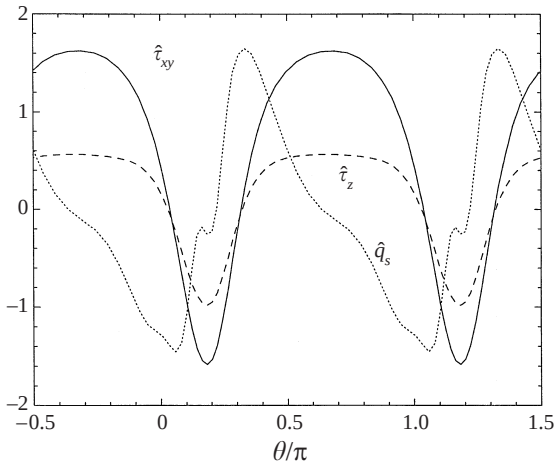

FIGURE 5. Distribution of the reduced in-plane shear tensions τ_{xy} and τ_z (solid and dashed line respectively), and of the transverse shear tension q_s (dotted line), along the trace of the capsule in the (x, y)-plane at equilibrium, plotted with respect to the polar angle θ for $\lambda = 1$, $G = 0.20$, and $\hat{\kappa}_B = 0.15$.

the reduced frequency $\hat{f} \equiv 4\pi/(kT)$ toward the value of unity corresponding to a rotating solid sphere.

Figure 5 illustrates the distribution of the in-plane shear tensions τ_{xy} and τ_z in the (x, y)-plane drawn, respectively, with the solid and dashed line, and of the transverse shear tension q_s drawn with the dotted line, for $\lambda = 1$, $G = 0.20$, and $\hat{\kappa}_B = 0.15$, at equilibrium. The reduced tensions, denoted by a caret are defined as $\hat{\tau}_{xy} \equiv \tau_{xy}/(\mu k a_{eq})$, $\hat{\tau}_z \equiv \tau_z/(\mu k a_{eq})$, and $\hat{q}_s \equiv q_s/(\mu k a_{eq})$, and are plotted with respect to the polar angle measured in the counterclockwise direction around the capsule centre. The distributions of the in-plane tensions are similar, but not identical, to those presented by Pozrikidis (1995) and Ramanujan & Pozrikidis (1998) in the absence of bending moments. The similarity occurs because the constitutive equation for the bending moments adopted in the present study does not introduce antisymmetric tensions, and the elastic tensions are determined solely by the instantaneous capsule shape. The graphs in figure 5 show that the magnitude of the transverse shear tensions is comparable to that of the elastic tensions, and reveal that compressive transverse tensions may develop near the point of maximum elongation.

Similar results were obtained for viscosity ratio $\lambda = 5$ where the capsules have more compact asymptotic shapes. The graphs in figure 6 illustrate the effect of the bending modulus on the equilibrium shape and transient deformation and orientation at the dimensionless shear rate $G = 0.05$. The high viscosity of the capsule restricts the deformation, as it does in the case of liquid drops with constant surface tension, and renders the effect of bending moments less significant. From a computational standpoint, the requirement on time step for numerical stability, combined with the need to solve an integral equation by iteration, raises the cost of these simulations to several days of CPU time on the aforementioned computing facilities, which is a serious pragmatic constraint.

6.2. *Biconcave disks*

Next, we consider the deformation of capsules with the initial shape of a biconcave disk whose trace in a meridional plane is described by equation (5.5). The initial

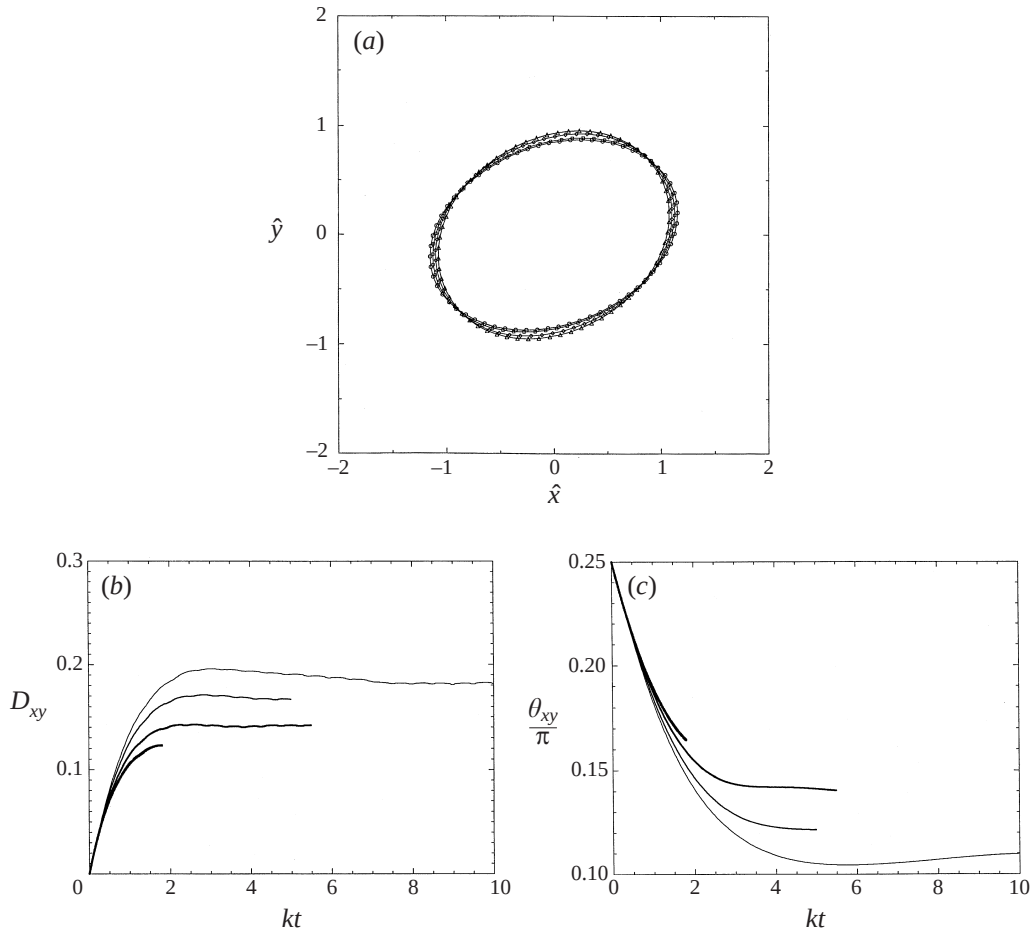

FIGURE 6. (*a*) Equilibrium shapes of capsules with viscosity ratio $\lambda = 5$ at dimensionless shear rate $G = 0.05$, for $\hat{\kappa}_B = 0, 0.01, 0.025$, and 0.0375. (b, c) Evolution of the Taylor deformation parameter and orientation in the (x, y)-plane; the thickness of the lines increases as the bending modulus is raised.

shape is also the reference shape of the membrane elastic tensions, which means that the initial elastic tensions vanish. Because, however, the reference shape concerning the bending moments is assumed to be a planar sheet, the initial transverse shear tensions are non-zero, and the equilibrium shape of the capsule is not the biconcave disk but a more rounded shape determined by the dimensionless bending modulus $\hat{\kappa}_B$. As $\hat{\kappa}_B$ is raised, the equilibrium shape tends to become spherical.

The equilibrium shape in hydrostatics is the sensible choice for the initial shape in the numerical simulations. Unfortunately, the accurate computation of this shape as the asymptotic limit of a relaxing capsule in the absence of an imposed flow was prevented by difficulties related to numerical instability, even when the motion was computed using the more efficient code for axisymmetric flow. Numerical experimentation indicated that the dimple of the biconcave disks disappears when $\hat{\kappa}_B$ is on the order of 0.01.

Figure 7 shows stages in the deformation of a capsule with $\lambda = 1$, initially inclined at 45° with respect to the x-axis, at dimensionless shear rate defined with respect to

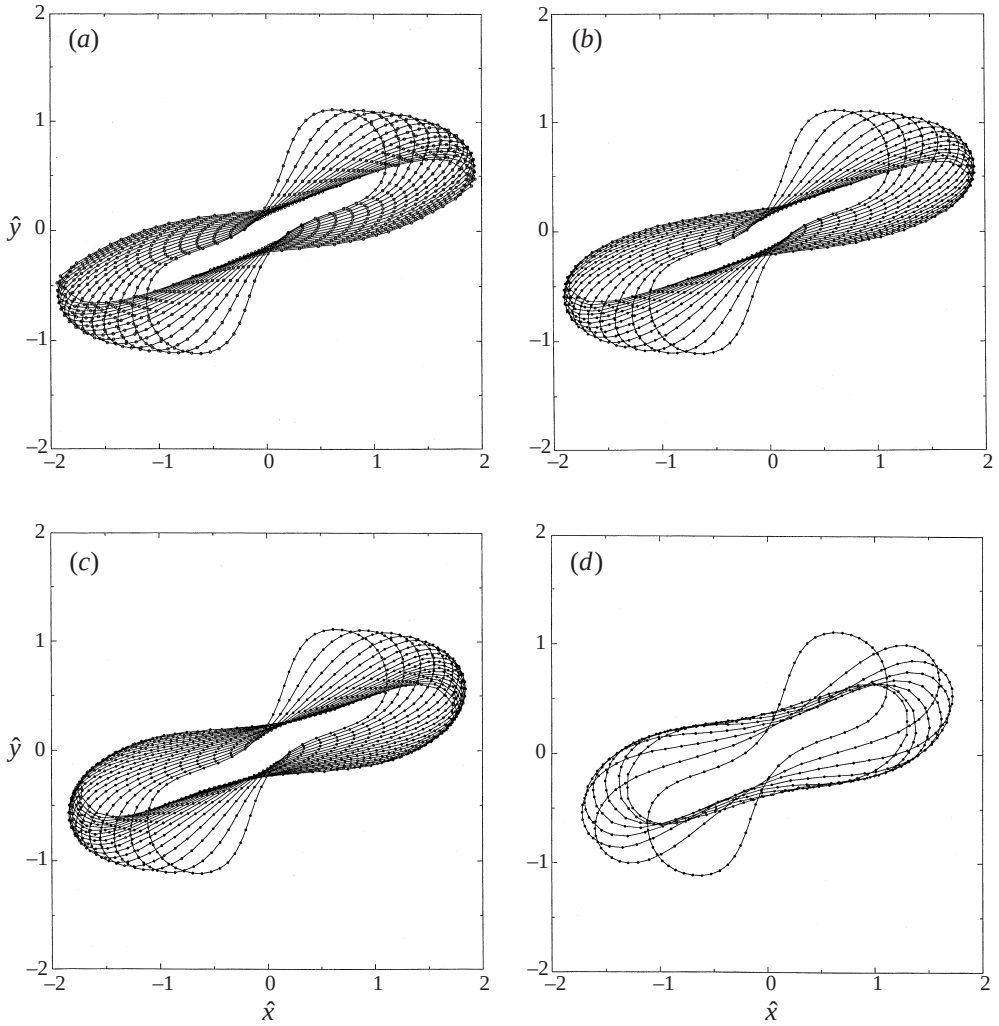

FIGURE 7. Stages in the deformation of a biconcave capsule with $\lambda = 1$, initially inclined at 45° with respect to the x-axis, at dimensionless shear rate $G = 0.20$, for (*a*) $\hat{\kappa}_B = 0$, (*b*) 0.002, (*c*) 0.001, and (*d*) 0.04.

the equivalent volume radius $G = 0.20$, for bending modulus $\hat{\kappa}_B = 0.0$, 0.002, 0.001, and 0.04. The results for $\hat{\kappa}_B = 0$ duplicate, and are in agreement with, those presented by Ramanujan & Pozrikidis (1998). At low values of $\hat{\kappa}_B$ the deformed capsule has a sigmoidal shape, whereas at high values the capsule tends to obtain the shape of an inclined oblate ellipsoid. The simulations ended when numerical instabilities developed near the region of maximum deformation due to the high curvature of the membrane. In spite of this limitation, the rounding effect of the membrane bending stiffness, locally at the tips and globally on the overall shape of the capsule, is apparent.

Ramanujan & Pozrikidis (1998) discussed the effect of the capsule resting-shape aspect ratio on the behaviour at long times. Simulations for oblate spheroidal capsules and biconcave disks with $\lambda = 1$ suggested that the capsules deform and obtain nearly stationary shapes while undergoing moderate shape oscillations, with the membrane

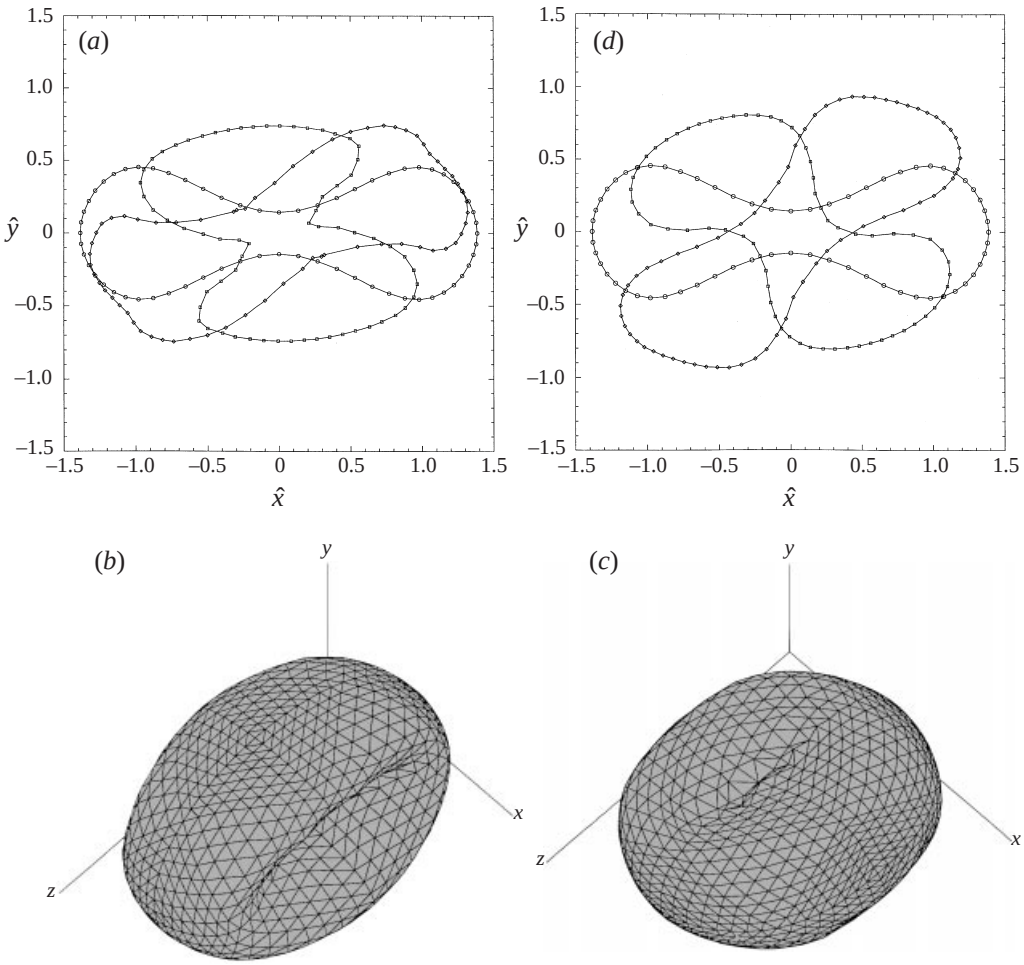

FIGURE 8. (*a*) Stages in the deformation of a biconcave capsule with $\lambda = 5$ initially aligned with the x-axis, at the dimensionless shear rate $G = 0.20$, in the absence of bending moments at times $kt = 0$ (○), 5.2 (□), and 9.2 (◇). (*b*, *c*) Three-dimensional perspectives at times $kt = 5.0$ and 9.3, illustrating transient membrane folding. (*d*) Same as (*a*) but for $\hat{\kappa}_B = 0.01$, at times $kt = 0$, 4.35, and 7.29, corresponding, respectively, to the circles, squares, and diamonds.

rotating around the capsule in a tank-treading mode. As the aspect ratio of the resting shape in increased, the amplitude and period of the oscillations are both raised. The results presented in figure 7 suggest that bending stiffness does not affect the nature of the motion at long times documented in the earlier study.

Figure 8 shows results of a more demanding set of simulations with $\lambda = 5$ at dimensionless shear rate $G = 0.20$. At the initial instant, the mid-plane of the biconcave disk lies in the (z, x)-plane. Figure 8(*a*) shows a sequence of evolving capsule contours in the (x, y)-plane in the absence of bending stiffness corresponding to $\hat{\kappa}_B = 0$, at dimensionless times $kt = 0$, 5.2, and 9.2. Figure 8(*b*, *c*) shows three-dimensional perspectives of the capsule shape at dimensionless times $kt = 5.0$ and 9.3, illustrating significant transient membrane folding. The numerical investigations of Ramanujan & Pozrikidis (1998) indicated that, as the viscosity ratio λ is raised, a transition occurs in the capsule's behaviour: steady deformation accompanied by

shape oscillations is gradually replaced by global rotation similar to that exhibited by non-spherical rigid particles (Jeffery 1922); in the case of capsules, global rotation is accompanied by membrane tank-treading motion. Transition from shape oscillation to global rotation is discernible in the profiles shown in figure 8(*a*).

The effect of bending stiffness becomes evident by comparing the profiles shown in figure 8(*a*) with those shown in figure 8(*d*) corresponding to identical conditions except that $\hat{\kappa}_B = 0.01$. Transient membrane folding is suppressed, and the capsule rotates with less deformation, developing bulged shapes on either end. Thus, bending stiffness promotes the transition to the Jeffery mode by forcing the capsule to project deeper into the streamlines of the incoming simple shear flow.

7. Discussion

We have discussed a Cartesian formulation for describing elastic tensions and bending moments developing in a thin membrane regarded as a thin shell; we have derived differential and integral force and torque balances involving membrane tensions, membrane moments, and hydrodynamic tractions acting as a distributed load; and we have presented numerical implementations based on boundary element methods.

Results of numerical simulations conducted by the boundary element method for capsules with spherical and biconcave unstressed shapes deforming under the influence of simple shear flow confirmed that the membrane stiffness restrains the overall capsule deformation and leads to more compact equilibrium shapes at long times. In the case of membranes consisting of thin elastic sheets, bending moments arise in the process of integrating the membrane stresses over the small but non-infinitesimal cross-section of the interfacial stratum; accordingly, the present numerical results effectively illustrate the significance of the non-infinitesimal membrane thickness. For membranes consisting of molecular networks, the numerical results illustrate the effect of stiffness of the three-dimensional interfacial bonds.

Consideration of the effect of bending moments was motivated, in part, by a desire to develop an integrated model for describing the deformation of red blood cells, accounting for the effect of membrane bending stiffness. Previous authors have accounted for the effects of in-plane elastic tensions, membrane viscosity, and membrane incompressibility, as discussed in the Introduction. The ratio of the viscosity of the red blood cell interior fluid to the viscosity of the suspending fluid *in vivo* ranges betwen 5 and 10. The modulus of elasticity of the healthy red cell membrane is on the order of $E_S = 10^{-3}\,\mathrm{dyn\,cm^{-1}}$, and the bending modulus is on the order of $\kappa_B = 10^{-12}\,\mathrm{dyn\,cm}$ (e.g. Zarda *et al.* 1973; Lipowsky 1991). Taking the equivalent volumetric radius of the cell to be $a_{eq} \simeq 3.0\,\mu\mathrm{m}$, we find that the reduced bending modulus $\hat{\kappa}_B \equiv \kappa_B/(a_{eq}^2 E_S)$ is on the order of 10^{-2}, corresponding to the motion depicted in figure 8(*d*).

The requirement of surface incompressibility on membranes consisting of lipid bilayers is responsible for the development of isotropic tensions that have not been included in the present formulation. For the evolutions displayed in figure 8, the total surface area of the membrane is reduced by 10% during the motion. Bending moments and isotropic tensions ensuring incompressibility are believed to play a central role in hydrostatics by determining, and providing an explanation for, the biconcave shape of red cells and for the more involved shapes of vesicles. Equilibrium axisymmetric shapes have been discussed and computed by several previous authors using a direct formulation or a formulation in terms of the bending energy function

(e.g. Zarda *et al.* 1977; Seifert *et al.* 1991; Seifert 1997). An alternative methodology particularly suited for three-dimensional shapes is suggested by the Cartesian formulation discussed in this work.

The successful implementation of the equations of shell mechanics in global Cartesian coordinates using standard numerical methods encourages its adaptation to other problems of biofluiddynamics involving fluid–structure interaction. Pedley and Heil studied steady flow through a flexible fluid-carrying elastic tube collapsed in a non-axisymmetric fashion due to negative transmular pressure (e.g. Heil 1997; Pedley & Luo 1998). To set up a realistic model for the wall mechanics, a nonlinear shell theory in which elastic tensions and bending moments arise from a strain-energy function by means of the principle of virtual displacements for infinitesimal variations was employed. Justification for the use of the small displacement theory is provided by the physical observation that, in spite of the large deformations, the strains of the shell are small, and the use of Hooke's law and Love's approximation for the strain-energy function in terms of the strain and bending energy tensors are appropriate (Heil & Pedley 1995). The wall was assumed to be unstressed in the cylindrical state, and the equations of shell mechanics were developed in surface curvilinear coordinates.

The present formulation offers an alternative for modelling the wall mechanics in Cartesian coordinates, relaxing the assumption of small deformations. An important restriction is the requirement that the resting shape has uniform curvature. For arbitrary resting shapes, the formulation in terms of surface curvilinear coordinates implemented either directly by force and torque balances or indirectly in terms of the principle of virtual displacements developed by Pedley and Heil appears to be the only alternative. This, however, may not be a serious limitation: cylindrical membranes readily arise from the rolling of flat sheets.

This research has been supported by a grant provided by the National Science Foundation.

REFERENCES

Barthès-Biesel, D. 1980 Motion of spherical microcapsule freely suspended in a linear shear flow. *J. Fluid Mech.* **100**, 831–853.

Barthès-Biesel, D. & Rallison, J. M. 1981 The time-dependent deformation of a capsule freely suspended in a linear shear flow. *J. Fluid Mech.* **113**, 251–267.

Boey, S. K., Boal, D. H. & Discher, D. E. 1998 Simulations of the erythrocyte cytoskeleton at large deformation. I. Microscopic models. *Biophys. J.* **75**, 1573–1583.

Canham, P. B. 1970 The minimum energy of bending as a possible explanation of the biconcave shape of the human red blood cell. *J. Theor. Biol.* **26**, 61–81.

Chang, K. S. & Olbricht, W. L. 1993*a* Experimental studies of the deformation of a synthetic capsule in extensional flow. *J. Fluid Mech.* **250**, 587–608.

Chang, K. S. & Olbricht, W. L. 1993*b* Experimental studies of the deformation and breakup of a synthetic capsule in steady and unsteady simple shear flow. *J. Fluid Mech.* **250**, 609–633.

Discher, D. E., Boal, D. H. & Boey, S. K. 1998 Simulations of the erythrocyte cytoskeleton at large deformation. II. Micropipette aspiration. *Biophys. J.* **75**, 1584–1597.

Eggleton, C. D. & Popel, A. S. 1998 Large deformation of red blood cell ghosts in simple shear flow. *Phys. Fluids* **10**, 1834–1845.

Evans, E. A. & Fung, Y. C. 1972 Improvement of measurements of the erythrocyte geometry. *Microvasc. Res.* **4**, 335–347.

Fung, Y. C. 1965 *Foundations of Solid Mechanics.* Prentice-Hall.

Fung, Y. C. 1981 *Biomechanics; Mechanical Properties of Living Tissues.* Springer.

Heil, M. 1997 Stokes flow in collapsible tubes: computation and experiment. *J. Fluid Mech.* **353**, 285–312.

Heil, M. & Pedley, T. J. 1995 Large axisymmetric deformation of a cylindrical shell conveying a viscous flow. *J. Fluids Struct.* **9**, 237–256.

Helfrich, W. 1973 Elastic properties of lipid bilayers: theory and possible experiments. *Naturforsch* **28**, 693–703.

Jeffery, G. B. 1922 The motion of ellipsoidal particles immersed in a viscous fluid. *Proc. R. Soc. Lond.* A **102**, 161–179.

Kraus, M., Wintz, W., Seifert, U. & Lipowsky, R. 1996 Fluid vesicles in shear flow. *Phys. Rev. Lett.* **77**, 3685–3688.

Kwak, S. & Pozrikidis, C. 2001 Effect of membrane bending stiffness on the deformation of capsules in axisymmetric extensional flow. *Phys. Fluids* **13**, 1234–1242.

Libai, I. & Simmonds, J. G. 1998 *The Nonlinear Theory of Elastic Shells.* Cambridge University Press.

Lipowsky, R. 1991 The conformation of membranes. *Nature* **349**, 475–481.

Navot, Y. 1998 Elastic membranes in viscous shear flow. *Phys. Fluids* **10**, 1819–1833.

Pedley, T. J. & Luo, X. Y. 1998 Modelling flow and oscillations in collapsible tubes. *Theor. Comput. Fluid Dyn.* **10**, 277–294.

Pozrikidis, C. 1992 *Boundary Integral and Singularity Methods for Linearized Viscous Flow.* Cambridge University Press.

Pozrikidis, C. 1995 Finite deformation of liquid capsules enclosed by elastic membranes in simple shear flow. *J. Fluid Mech.* **297**, 123–152.

Pozrikidis, C. 2001 Interfacial dynamics for Stokes flow. *J. Comput. Phys.* **169**(2) (In press).

Ramanujan, S. & Pozrikidis, C. 1998 Deformation of liquid capsules enclosed by elastic membranes in simple shear flow: large deformations and the effect of fluid viscosities. *J. Fluid Mech.* **361**, 117–143.

Seifert, U. 1997 Configurations of fluid membranes and vesicles. *Adv. Phys.* **46**, 13–137.

Seifert, U., Berndl, K. & Lipowsky, R. 1991 Shape transformations of vesicles: Phase diagram for spontaneous curvature and bilayer-coupling models. *Phys. Rev.* A **361**, 117–143.

Steigmann, D. J. 1999 Fluid films with curvature elasticity. *Arch. Rat. Mech.* **150**, 127–152.

Steigmann, D. J. & Ogden, R. W. 1997 Plane deformations of elastic solids with intrinsic boundary elasticity. *Proc. R. Soc. Lond.* A **453**, 853–877.

Steigmann, D. J. & Ogden, R. W. 1999 Elastic surface-substrate interactions. *Proc. R. Soc. Lond.* A **455**, 427–474.

Timoshenko, S. & Woinowsky-Krieger, S. 1959 *Theory of Plates and Shells.* McGraw-Hill.

Walter, A., Rehage, H. & Leonhard, H. 2000 Shear-induced deformations of polyamide microcapsules. *Colloid Polymer Sci.* **278**, 169–175.

Valid, R. 1995 *The Nonlinear Theory of Shells through Variational Principles.* Wiley.

Zarda, P. R., Chien, S. & Skalak, R. 1997 Elastic deformations of red blood cells. *J. Biomechanics* **10**, 211–221.